



Molecular Physics

An International Journal at the Interface Between Chemistry and Physics

ISSN: (Print) (Online) Journal homepage: <https://www.tandfonline.com/loi/tmph20>

Infrared photodissociation spectroscopy of D₂-tagged CH₃CO₂⁻(H₂O)₀₋₂ anions

Jessalyn A. DeVine , Sreekanta Debnath , Ya-Ke Li , Laura M. McCaslin , Wieland Schöllkopf , Daniel M. Neumark & Knut R. Asmis

To cite this article: Jessalyn A. DeVine , Sreekanta Debnath , Ya-Ke Li , Laura M. McCaslin , Wieland Schöllkopf , Daniel M. Neumark & Knut R. Asmis (2020) Infrared photodissociation spectroscopy of D₂-tagged CH₃CO₂⁻(H₂O)₀₋₂ anions, Molecular Physics, 118:11, e1749953, DOI: [10.1080/00268976.2020.1749953](https://doi.org/10.1080/00268976.2020.1749953)

To link to this article: <https://doi.org/10.1080/00268976.2020.1749953>

 View supplementary material 

 Published online: 17 Apr 2020.

 Submit your article to this journal 

 Article views: 87

 View related articles 

 View Crossmark data 

Infrared photodissociation spectroscopy of D₂-tagged CH₃CO₂⁻(H₂O)_{0–2} anions

Jessalyn A. DeVine^a, Sreekanta Debnath^{b,c}, Ya-Ke Li^{b,c}, Laura M. McCaslin^{d,e}, Wieland Schöllkopf^{b,c}, Daniel M. Neumark^{b,a,f} and Knut R. Asmis^b

^aDepartment of Chemistry, University of California, Berkeley, CA, USA; ^bWilhelm-Ostwald-Institut für Physikalische und Theoretische Chemie, Universität Leipzig, Leipzig, Germany; ^cFritz-Haber-Institut der Max-Planck-Gesellschaft, Berlin, Germany; ^dInstitute of Chemistry and the Fritz Haber Center for Molecular Dynamics, The Hebrew University, Jerusalem, Israel; ^eDepartment of Chemistry, University of California, Irvine, CA, USA; ^fChemical Sciences Division, Lawrence Berkeley National Laboratory, Berkeley, CA, USA

ABSTRACT

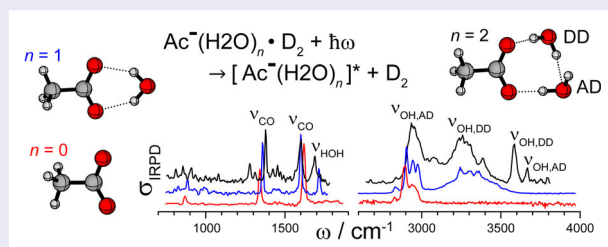
Infrared photodissociation spectroscopy of D₂-tagged anions is used to obtain the vibrational spectra of microsolvated acetate, CH₃CO₂⁻(H₂O)_n (*n* = 0–2), in the CH/OH stretching (~4000–2500 cm⁻¹) and fingerprint (~1800–800 cm⁻¹) spectral regions. These results are analysed by comparison to anharmonic IR spectra from MP2 calculations as well as Born-Oppenheimer molecular dynamics (BOMD) simulations. In agreement with prior work, we find that the first water molecule adds to the acetate anion by donating two hydrogen bonds, yielding a symmetrical structure involving a six-membered hydrogen-bonded ring. Two nearly degenerate binding motifs that differ in energy by less than 1 kJ/mol are identified for *n* = 2 anion, where the lowest-energy geometry has two ion-water hydrogen bonds as well as a water-water hydrogen bond. The molecular dynamics simulations confirm that this lower-energy structure is preferred over a slightly higher-lying configuration possessing three ion-water hydrogen bonds and no water-water interactions. Analysis of the molecular motion contributing to peaks in the BOMD spectra via a generalised normal mode approach provides assignment of all observed transitions to the lower-energy structure, and enables distinction of the vibrational signatures associated with ion-water and water-water intermolecular motions.

ARTICLE HISTORY

Received 30 January 2020
Accepted 19 March 2020

KEYWORDS

Ion spectroscopy; vibrational spectroscopy; infrared photodissociation; microsolvation



1. Introduction

The carboxylic acid group (–CO₂H) is a common substructure found in biomolecules such as amino and fatty acids. The local solvation environment can play a key role in determining the chemical and biological behaviour of such molecules, in part due to its impact on the protonation state of the acid group. At a typical *in vivo* pH (~7), carboxylic acids are found primarily in the deprotonated RCO₂⁻ state [1], so the geometry of the solvation shell surrounding carboxylate anions is important for

biomolecular interactions and protein structures [2–6]. Among the simple carboxylate ions, acetate (R = CH₃) is the smallest which possesses a hydrophobic group, providing the simplest model for the types of mixed hydration interactions prevalent in biomolecules where relatively extensive hydrophobic regions are interspersed with polar functional groups. In this work, the evolution of a solvation shell around the acetate anion is considered by using infrared (IR) action spectroscopy [7–12] as a structural probe of CH₃CO₂⁻(H₂O)_n anions

CONTACT Daniel M. Neumark  dneumark@berkeley.edu  Department of Chemistry, University of California, Berkeley, CA 94720, USA, Chemical Sciences Division, Lawrence Berkeley National Laboratory, Berkeley, CA 94720, USA; Knut Asmis  knut.asmis@uni-leipzig.de  Wilhelm-Ostwald-Institut für Physikalische und Theoretische Chemie, Universität Leipzig, Linnéstrasse 2, 04103 Leipzig, Germany

 Supplemental data for this article can be accessed here. <https://doi.org/10.1080/00268976.2020.1749953>

($n = 0-2$), providing insight into the structures and dynamics involved in microhydration of a simple carboxylate anion.

The bulk solvation of the first three homologous carboxylate anions RCO_2^- ($\text{R} = \text{H}, \text{CH}_3, \text{CH}_2\text{CH}_3$) has been investigated using IR spectroscopy of aqueous sodium carboxylate solutions [13], where HDO was used as a probe of the solvation environment surrounding the RCO_2^- anions. It was found that interaction of the solvent molecules with the carboxylate group imposes an asymmetric electronic distribution, where the extent of asymmetry is dependent on the electron-donating ability of the substituent group R. While this work demonstrated that larger hydrophobic groups result in a more asymmetric ion-water interaction, it is limited in its ability to provide detailed structural information regarding the binding motifs present in the first solvation shell. One experimental approach to the structural characterisation of microsolvated conjugate bases is gas-phase spectroscopy of size-selected anions, which allows for stepwise addition of solvent molecules to ions that are prevalent in aqueous media [8]. The two best-established methods for characterisation of gas phase cluster ions are anion photoelectron spectroscopy [14] and infrared action spectroscopy [8–12]. Anion photoelectron spectra have been obtained for microhydrated acetate $\text{Ac}^-(\text{H}_2\text{O})_n$ ($n = 0-3$) by Wang and coworkers; [15] however, these photoelectron spectra lack vibrational resolution and thus structural information on these anions is limited.

IR action spectroscopy based upon electron ejection and subsequent capture by a scavenger (SF_6) has been used to probe the vibrational spectrum of room temperature Ac^- in the $700-1700\text{ cm}^{-1}$ frequency range [16]. This spectrum showed three broad features ($\sim 100\text{ cm}^{-1}$ FWHM) at $1590, 1305, \text{ and } 835\text{ cm}^{-1}$ that were assigned to the antisymmetric and symmetric carboxylate stretching and the OCO bending modes, respectively. IR action spectroscopies based on messenger-tagging typically require cooling of the ions to cryogenic temperatures in order for the weakly-bound tagged ions to remain intact between formation and spectral interrogation [9,17,18]. The inherent low temperature of these experiments assists in structural assignment of the probed ions, particularly in cases where multiple low-energy isomers exist, and greatly reduces rotational broadening. This approach has been used by Johnson and coworkers to probe the evolution of a solvation shell around several RCO_2^- anions [19,20]. Particular attention has been paid to the monohydrate of the acetate anion, $\text{Ac}^-(\text{H}_2\text{O})$ [21,22], where the loss of an Ar tag was monitored as a function of photon energy to obtain the vibrational spectrum in the OH/CH stretching region ($\sim 3800-2800\text{ cm}^{-1}$). These

results showed that the first water molecule donates two hydrogen bonds to the acetate anion. Particularly in the OH stretching region, a harmonic analysis of the IR spectrum of this double donor (DD) motif failed to adequately describe the observed spectrum, and an adiabatic model was introduced to describe coupling between the OH stretching modes and a low-frequency intermolecular (IM) rocking mode.

In the current work, infrared photodissociation (IRPD) spectra of D_2 -tagged Ac^- , $\text{Ac}^-(\text{H}_2\text{O})$, and $\text{Ac}^-(\text{H}_2\text{O})_2$ are presented over a broad spectral range ($4000-800\text{ cm}^{-1}$), covering the OH/CH stretching ($4000-2500\text{ cm}^{-1}$) as well as the fingerprint ($1800-800\text{ cm}^{-1}$) spectral regions. The spectra are assigned based on a comparison to anharmonic MP2/aug-cc-pVDZ frequencies and intensities of low energy isomers and molecular dynamics simulations, when necessary. These results are compared to those found for several other ions with similar substructures, as well as the aqueous IR spectrum of Ac^- [23].

2. Experimental methods

IRPD experiments are performed using a cryogenic ion trap tandem mass spectrometer described previously [24,25]. In brief, microhydrated acetate anions, $\text{Ac}^-(\text{H}_2\text{O})_n$, are continuously generated in a modified Z-spray ionisation source using a 10 mM aqueous solution of sodium acetate in pure distilled water. Anions pass through a 4-mm diameter skimmer and are collimated in a radio frequency (RF) decapole ion-guide. The ions are then mass-selected with a quadrupole mass-filter, deflected 90° by an electrostatic quadrupole deflector, and focused into a cryogenic RF ring-electrode ion trap [24].

The trap is held at 20 K and continuously filled with a D_2/He buffer gas mixture; a 5% D_2 gas mixture was used to tag the Ac^- anion, whereas a 25% mixture was used for tagging $\text{Ac}^-(\text{H}_2\text{O})$ and $\text{Ac}^-(\text{H}_2\text{O})_2$. The mass distributions of ions obtained with and without D_2 in the trap are provided in Figure S1 of the Supporting Information (SI). During their residence time in the trap, collisions with the buffer gas gently cool the ions' internal degrees of freedom and typically avoid the production of kinetically trapped species, although there are exceptions [26]. At sufficiently low ion-trap temperatures, ion-messenger complexes with D_2 are formed via three-body collisions [17].

The ions are accumulated in the trap either for 100 ms or 200 ms, depending on the IR laser used, then extracted and focused both temporally and spatially into the extraction region of an orthogonal time-of-flight (TOF) mass spectrometer. Here, the ions are irradiated

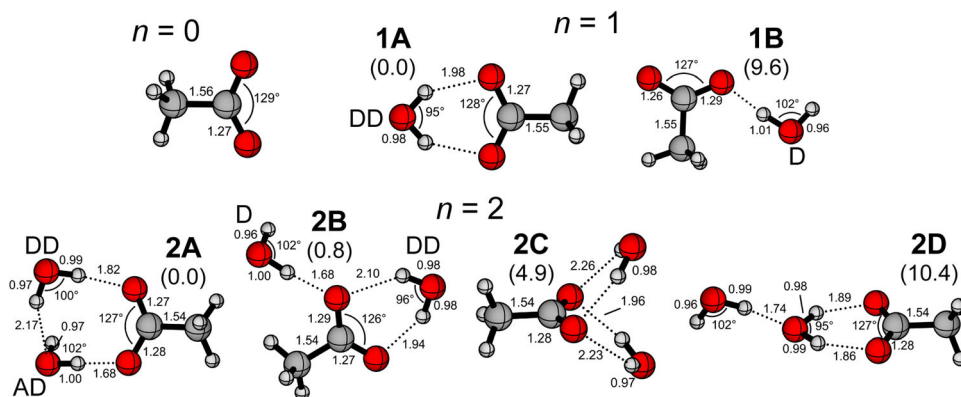


Figure 1. Optimised MP2/aug-cc-pVDZ geometries for the $\text{Ac}^-(\text{H}_2\text{O})_n$ anions. Relative energies (ΔE^0) are provided in units of kJ/mol, and bond lengths are provided in angstroms.

with a counter-propagating beam of an IR laser pulse generated either by the Fritz-Haber-Institute Free Electron laser (FHI FEL) [27] or a table-top OPO/OPA laser system [28]. For the lower-energy spectral range (1800–800 cm^{-1}), the FHI FEL was used to generate laser pulses with a spectral resolution $\Delta\lambda/\lambda \cong 0.5\%$ FWHM and attenuated pulse energies of 2–6 mJ at 5 Hz repetition rate. The OPO/OPA laser, operating at 10 Hz, provided access to frequencies ranging from 4000–2500 cm^{-1} with pulse energies of 2–8 mJ. In both energy regions, the laser beam was attenuated in order to minimise multi-photon excitation.

Following the interaction with the IR laser pulse, all parent and photofragment ions are accelerated towards a microchannel plate detector and monitored as a function of irradiated wavelength. IRPD scans are recorded by averaging over 100 time-of-flight mass spectra per wavelength step (4 cm^{-1} for the FHI FEL and 3 cm^{-1} for the OPO/OPA system). Typically, at least three scans are summed to obtain the final IRPD spectrum. The IRPD cross section, σ_{IRPD} , is obtained as described previously [29,30].

3. Computational methods

3.1. Electronic structure and frequency calculations

Optimised geometries as well as harmonic and VPT2 vibrational frequencies and intensities for the bare and D_2 -tagged $\text{Ac}^-(\text{H}_2\text{O})_n$ ($n = 0$ –2) anions were obtained at the MP2/aug-cc-pVDZ level of theory using the programme package Gaussian 16 [31–33]. A single structure was assumed for the $n = 0$ anion. For anions with one and two water molecules, several isomers were considered, and each final geometry was confirmed as a local energy minimum through a harmonic frequency analysis. The resulting geometries are shown in Figure 1

and discussed in more detail below. These were then re-optimised to include a D_2 tag; the resultant Cartesian coordinates for the low-energy D_2 -tagged structures of each stoichiometry are provided in Tables S1–S3 of the SI. The MP2 harmonic spectra are provided in Figures S2–S4 in the SI. Anharmonic frequency calculations were performed for the D_2 -tagged ions using second-order vibrational perturbation theory (VPT2) [34] and are discussed in more detail in Section 5. For the low-energy geometries of each anion, harmonic and anharmonic vibrational frequencies and fundamental intensities are presented in Tables S4–S8 of the SI.

To obtain more reliable energies, CCSD(T)/aug-cc-pVTZ single-point calculations were performed at each of the MP2/aug-cc-pVDZ optimised geometries for the D_2 -tagged $n = 0$ –2 anions, as well as the D_2 and H_2O molecules [32,35,36]. The CCSD(T)/aug-cc-pVDZ and CCSD(T)/aug-cc-pVTZ energies were corrected using the MP2/aug-cc-pVDZ zero-point energies (ZPEs), yielding the relative energies (ΔE^0), D_2 binding energies (ΔE_{D_2}), and water binding energies (ΔE_{wat}) provided in Tables S9–S11 of the SI. Unless otherwise indicated, all energies quoted in the following sections are derived from the CCSD(T)/aug-cc-pVTZ zero-point corrected energies, ΔE^0 .

3.2. Molecular dynamics simulations

To consider the dynamical nature of the hydrogen bonds involved in the $n = 2$ anion, Born-Oppenheimer molecular dynamics (BOMD) trajectories were obtained starting from each of the two lowest-energy isomers **2A** and **2B** using QChem version 5.1 [37]. For each isomer, ten trajectories were calculated using the $\omega\text{B97X-D}/6\text{-}31 + \text{G}^*$ method [38–41]. The Nosé-Hoover thermostat [42] was used to maintain a constant temperature of 150 K throughout the simulation. While the experiments to

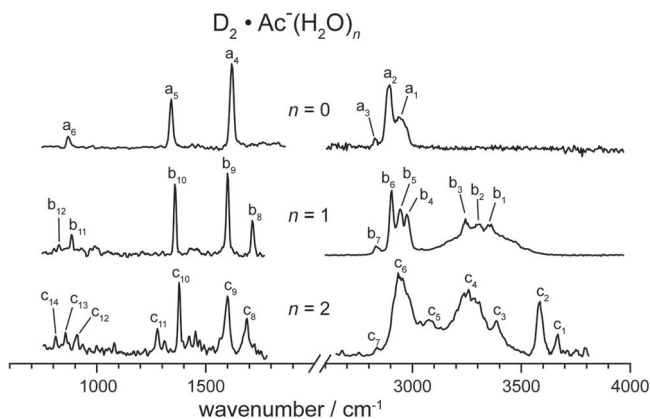


Figure 2. IRPD spectra of D_2 -tagged $Ac^-(H_2O)_n$ anions.

which these results are compared were performed at 20 K, a higher temperature was chosen for the BOMD simulations so that a shorter dynamical time window would show the nuclear motion of interest. Initial velocities were sampled from a Boltzmann velocity distribution, and initial geometries were taken to be the MP2/aug-cc-pVDZ optimised structures shown in Figure 1. Dynamics were propagated for 20,000 steps with a 20 au (~ 0.5 fs) time step, providing trajectories that span roughly 10 ps in time.

The spectral density and IR spectra were then obtained from the Fourier transform of the nuclear velocity and dipole-dipole autocorrelation functions, respectively. For trajectories where the initial water binding motif was preserved for the full dynamical time frame (all 10 runs for **2A**; runs 1, 2, and 6 for **2B**), the 5000–500 cm^{-1} region of the IR spectra and spectral densities were normalised, and the normalised average of these traces give the **2A** and **2B** BOMD spectra shown in Figure S5 of the SI. Analysis of peaks in the calculated IR spectrum was performed via correlation of the relevant molecular motion to regions of high spectral density, as described by Mathias and Baer [43].

4. Results

4.1. IRPD spectra

The IRPD spectra of D_2 -tagged $Ac^-(H_2O)_n$ ($n = 0, 1$ and 2) obtained by monitoring the D_2 -loss channel are shown in Figure 2 for the OH/CH stretching (4000 – 2600 cm^{-1}) and the fingerprint (1800 – 800 cm^{-1}) spectral regions. As noted above, the OH/CH stretching region of the Ar-tagged monohydrate anion has been previously observed by Johnson and coworkers; [21,22] this spectrum is shown along with the current results in Figure S6 of the SI.

Table 1. Peak positions, widths (cm^{-1}), and assignments for features in the IRPD spectrum of the D_2 -tagged acetate anion.

peak	cm^{-1}	FWHM	VPT2	desc.
a ₁	2945	63	2984; 2980	CH str.
a ₂	2891	33	2940	D_2 str.
a ₃	2831	26	2916	CH str.
a ₄	1620	20	1595	antisym. carboxylate str.
a ₅	1341	18	1350	sym. carboxylate str.
a ₆	870	18	859	OCO bend

Note: The corresponding VPT2 energies (cm^{-1}) are also provided.

The higher-energy region of the $n = 0$ spectrum shows three overlapping transitions (a₁, a₂, a₃) in the CH stretching region (~ 3000 – 2800 cm^{-1}) with relatively broad peak widths exceeding 20 cm^{-1} FWHM. The frequencies and intensities of the three features a₄ to a₆ are similar to the three transitions reported previously [16], identifying them as the antisymmetric (a₄) and symmetric (a₅) carboxylate stretching and OCO bending (a₆) modes (see Table 1). In our spectrum, these bands are much narrower (~ 10 cm^{-1} FWHM), representing a considerable improvement in resolution over the previous measurement arising from the lower internal temperature of the ions probed.

Addition of the first water molecule introduces a broad spectral feature with partially resolved structure (b_{1–3} in Figure 2) in the hydrogen-bonded OH stretching region (3650 – 3000 cm^{-1}) of the $n = 1$ spectrum. The observed progression with a spacing of ~ 60 cm^{-1} , previously reported by Johnson and coworkers [21,22], is characteristic for the water molecule adopting a DD binding motif, which leads to strong coupling of a low-frequency rocking mode with the water O-H oscillators. In the CH stretching region (3000 – 2800 cm^{-1}), the Ar-tagging experiment (Figure S6) showed three transitions, giving vibrational frequencies of 2980, 2953, and 2912 cm^{-1} for the CH stretching modes of this anion. Similar structure is found here, where the spectra show four peaks in the CH stretching region (b₄ through b₇). In the fingerprint region (1800 – 800 cm^{-1}), peaks are observed at similar positions as those seen in the $n = 0$ spectrum (b₉, b₁₀, b₁₁), suggesting a similar assignment as for a₄ through a₆ (see Table 1); several new transitions are also seen upon the addition of the first water molecule, including the features labelled b₈ and b₁₂.

In the $n = 2$ spectrum, two new narrow peaks (c₁, c₂) are observed, one in the free O-H region (c₁, > 3650 cm^{-1}) and the other in the weakly hydrogen-bonded O-H stretching region (c₂, 3650 – 3500 cm^{-1}). The remainder of the OH and CH stretching regions for this ion shows four broad overlapping peaks (c₃ through c₆) with a low-intensity shoulder (c₇) on the red edge.

The fingerprint region shows considerably more structure than is seen for $n = 0$ and 1, though the three intense features identified for $n = 1$ are also present here (c_8 , c_9 , c_{10}). A new intense feature (c_{11}) is found below these three peaks. A triplet of peaks (c_{12} , c_{13} , c_{14}) as well as additional weak features are observed below 1000 cm^{-1} , where transitions a_6 ($n = 0$), b_{11} and b_{12} ($n = 1$) were seen.

4.2. Energetics and minimum-energy geometries

Figure 1 shows the low-energy isomers identified as local MP2/aug-cc-pVDZ minima for $\text{Ac}^-(\text{H}_2\text{O})_n$ ($n = 0-2$); the corresponding geometries of the D_2 -tagged species are pictured in Figure S7. Previous work on the $n = 1$ anion [12,15,22] found that addition of the first water molecule to the acetate ion forms a symmetric DD hydrogen-bonded structure (**1A**, C_s symmetry) with $\text{O}\cdots\text{H}-\text{O}$ bond angles of $\sim 145^\circ$, which is confirmed to be the lowest-energy geometry by our calculated energies. The D_2 tag is not found to substantially change the energetics nor break the symmetry. Additionally, a low-lying isomer **1B** exhibiting a single donor (D) motif with a near-linear ($\text{O}\cdots\text{H}-\text{O}$ bond angle 174°) hydrogen bond is identified 10 kJ/mol (see Table S9) above **1A**. For the D_2 -tagged ions, this energetic ordering is maintained (**1B**· D_2 , +9 kJ/mol).

For $n = 2$, four low-energy minima are identified. The global minimum-energy structure is **2A**, where the second water molecule inserts into one of the ion-water H-bonds of **1A** yielding one water in a DD and the other in an acceptor/donor (AD) motif. Both ion-water hydrogen bonds are found to be near-linear, with $\text{O}\cdots\text{H}-\text{O}$ bond angles of $\sim 175^\circ$, whereas the water-water H-bond forms an $\text{O}\cdots\text{H}-\text{O}$ bond angle of $\sim 145^\circ$. The anion photoelectron spectrum of $\text{Ac}^-(\text{H}_2\text{O})_2$ [15] was previously analysed assuming an anion geometry corresponding to **2A**. Isomer **2B**, which contains one DD and one D water motif, is nearly degenerate in energy and lies less than 1 kJ/mol above **2A**. This small energy difference suggests the possibility of interconversion between the low energy isomers, which will be discussed in more detail below. Two other isomers, **2C** and **2D**, lie 5 and 10 kJ/mol, respectively, above the **2A** isomer. The D_2 tag does not substantially change the relative energies of these binding motifs (see Table S9).

4.3. BOMD simulations

Interconversion between isomers would impact the resultant spectra. This possibility was explored for $n = 2$ by performing ten molecular dynamics simulations starting from geometries **2A** and **2B** in Figure 1, with a total of 20

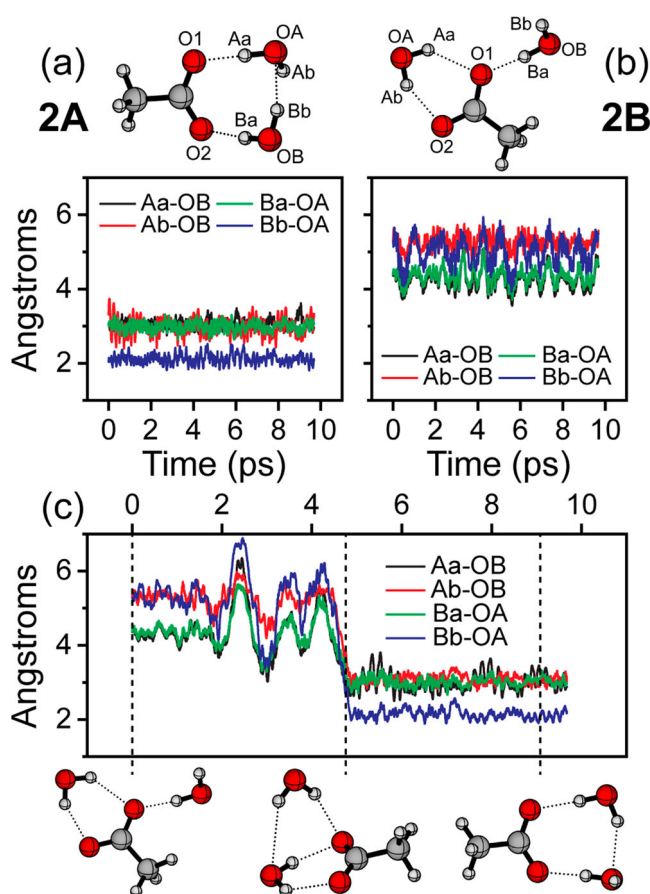


Figure 3. Typical water-water hydrogen bonding plots for BOMD trajectories starting from the **2A** (a) or **2B** (b) geometry, where the initial binding motif persists for the entire 10 ps run time. (c) Water-water O-H separations for a trajectory starting at the **2B** geometry which shows conversion to the **2A** binding motif, as well as snapshots of the molecular geometry before, during, and after the conformational change.

trajectories carried out to observe the structural changes over 10 ps. To analyze these trajectories for interconversion between the different water binding motifs, the intermolecular hydrogen-oxygen atom distance $r_{\text{O}\cdots\text{H}}$ is plotted as a function of time, using the labelling convention provided in Figure 3. The most useful metric for distinguishing between isomers **2A** and **2B** is the water-water hydrogen bond length in **2A**, $r_{\text{O(A)}\cdots\text{H(B)}}$ (or $r_{\text{O(B)}\cdots\text{H(A)}}$). Figure 3(a) shows the time evolution of all four intermolecular $r_{\text{O}\cdots\text{H}}$ distances for a typical trajectory starting from the **2A** geometry, and Figure 3(b) illustrates the behaviour that is observed when the **2B** binding motif is preserved over the 10 ps run time. In Figure 3(b), we see that the absence of a water-water hydrogen bond leads to larger fluctuations in the $r_{\text{O}\cdots\text{H}}$ distances for the **2B** isomer.

Figures S8–S11 in the SI provide a full summary of the intermolecular $\text{O}\cdots\text{H}$ separations for all 20 BOMD

trajectories. To summarise these results, all of the trajectories starting from the **2A** isomer show that the AD/DD binding motif persists for the full 10 ps of simulation, though the water/water hydrogen bond is not strictly static, with nine of the ten trajectories showing some reversal in the donor/acceptor role of the two waters. This role reversal is similar to that observed for the dihydrate of the iodide anion [44]. Of the ten trajectories initiated with the **2B** binding motif, seven show isomerisation to form the **2A** isomer after some period of time. This behaviour is illustrated in the hydrogen bonding plot of Figure 3(c). Of the 17 trajectories where the **2A** isomer is present – either through isomerisation from **2B**, or from the initial geometry – only a single trajectory shows conversion to another isomer, and this isomer is the high-energy **2D** structure. While it is possible that the presence of the D_2 tag may impact the propensity for interconversion, these results, as well as the fact that the relative energies are not changed by the D_2 tag, indicate that the $n = 2$ anion adopts the **2A** geometry independent of the presence of D_2 .

5. Spectral assignments

5.1. $n = 0$

Figure 4 compares the IRPD spectrum obtained for the D_2 -tagged Ac^- with the MP2/aug-cc-pVDZ/VPT2 anharmonic spectra. The two spectra show satisfactory agreement over the complete spectral range with some minor discrepancies. In the higher frequency region, the IRPD spectrum shows three broad overlapping features (a_1 , a_2 , a_3), whose relative intensities are well-reproduced by a 15 cm^{-1} FWHM convolution of the anharmonic stick spectrum. This choice of width is congruent with the relatively narrow features observed in the lower-energy spectral region for this anion. The broader feature in this region (a_1) likely encompasses the two antisymmetric CH stretching fundamentals. From the position of the fundamental transitions in the theoretical spectrum, we assign a_2 and a_3 to the D_2 stretch and symmetric CH stretching modes, respectively. The anharmonic simulation and convolution confirm that the observed broadening of these features relative to transitions observed in the lower-energy region of the spectrum arises from numerous low-intensity combination bands (shown as red sticks in Figure 4) involving the low-frequency D_2 wagging and CH_3 internal rotation modes.

In the lower-frequency region, the VPT2 results reproduce all three intense transitions, identifying peaks a_4 , a_5 , and a_6 as the antisymmetric carboxylate stretching, symmetric carboxylate stretching, and OCO bending fundamentals for the acetate anion, in agreement

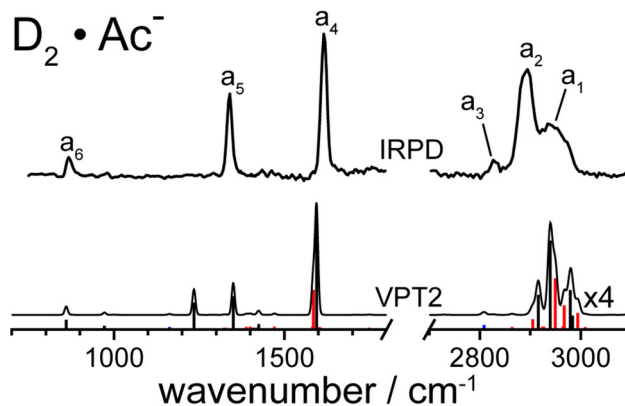


Figure 4. Comparison of the IRPD spectrum of the D_2 -tagged acetate anion (top) with the simulated spectrum obtained from a VPT2 treatment of the MP2/aug-cc-pVDZ minimum-energy geometry (bottom). The stick spectrum shows fundamental transitions, overtones, and combination bands as black, blue, and red sticks, respectively, and the solid black trace shows a convolution of this spectrum with a 15 cm^{-1} FWHM Gaussian lineshape. The $3100\text{--}2700\text{ cm}^{-1}$ region of the theoretical spectrum has been vertically scaled by the indicated factor for clarity. It should be noted that for the experimental spectrum, there is no direct relationship between the intensities in the two spectral ranges.

with the previous assignment [16]. The most notable discrepancy between experiment and the VPT2 results shown in Figure 4 is the simulated intense transition at $\sim 1220\text{ cm}^{-1}$. This transition corresponds to the CH_3 inversion fundamental, which has zero intensity in the harmonic spectrum (Figure S2). The cause of the anomalously high predicted intensity of this feature is unclear, but may be due to the tendency for VPT2 calculations to overestimate oscillator strengths in cases where there are nearly-degenerate vibrational levels.

5.2. $n = 1$

Figure 5 compares the IRPD spectrum for the $n = 1$ anion to the VPT2 spectra of **1A**· D_2 and **1B**· D_2 . The OH stretching region of both simulated spectra do not provide good agreement with experiment (peaks b_1 – b_3), congruent with prior analyses. As mentioned above, this is a result of strong coupling between the OH stretching modes and a low-frequency IM rocking motion in the **1A** isomer. The adiabatic model derived previously to describe this coupling [22] showed that the resultant OH stretching region of the vibrational spectrum displays a progression of features which correspond to excitation of one quantum of OH stretch and a range of quanta of the IM rocking mode. Thus, we assign the three peaks in the OH stretching region as peaks belonging to this progression, as summarised in Table 2.

The CH stretching region of the VPT2 spectrum provides better agreement with experiment, providing

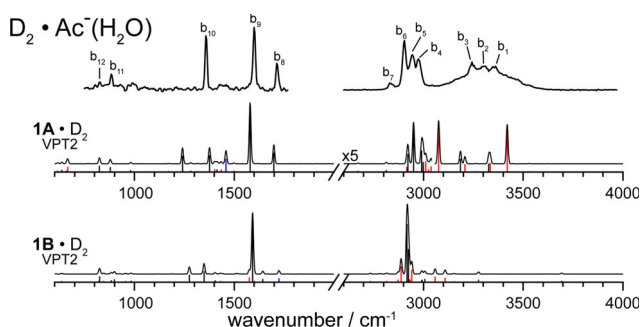


Figure 5. Comparison of the IRPD spectrum of D_2 -tagged $Ac^-(H_2O)$ (top) to the VPT2 simulations obtained for the two D_2 -tagged isomers identified in MP2/aug-cc-pVDZ calculations (bottom). The stick spectra show fundamental transitions, overtones, and combination bands as black, blue, and red sticks, respectively, and the solid black traces show a convolution of each spectrum with a 15 cm^{-1} FWHM Gaussian lineshape. The $3050\text{--}2600\text{ cm}^{-1}$ region of the $1A\cdot D_2$ spectrum has been vertically scaled by the indicated factor for clarity.

Table 2. Peak positions, widths (cm^{-1}), and assignments for features in the IRPD spectrum of the D_2 -tagged $Ac^-(H_2O)$ anion.

peak	cm^{-1}	FWHM	VPT2	desc.
b_1	3358	38	$3651 + 73m$	OH str. + $(m + 2)$ IM rock
b_2	3299	55	$3578 + 73m$	OH str. + $(m + 1)$ IM rock
b_3	3244	32	$3505 + 73m$	OH str. + m IM rock
b_4	2977	31	3000	antisym. CH str.
b_5	2942	31	2992	antisym. CH str.
b_6	2904	22	2923	sym. CH str.
b_7	2838	24	2814	HOH bend OT
b_8	1715	14	1701	HOH bend
b_9	1600	13	1581	antisym. carboxylate str.
b_{10}	1359	13	1377	sym. carboxylate str.
b_{11}	885	12	879	OCO bend
b_{12}	827	11	824	H_2O wag

Note: The corresponding VPT2 energies (cm^{-1}) are also provided. The variable m is used to indicate that the resolution of the current results does not provide definitive assignment of the three peaks belonging to the OH stretching anharmonic progression.

assignment of transitions b_4 , b_5 , and b_6 as CH stretching fundamentals, in agreement with results of the Ar tagging experiments [21]. Peak b_6 , which is assigned to the symmetric CH stretching fundamental, is slightly more intense than was observed in the Ar-tagging experiment, and the VPT2 results indicate that this is due to contributions from the D_2 stretching fundamental. In addition to the CH stretching features, the current results probe slightly lower frequencies, revealing an additional weak transition at 2838 cm^{-1} (b_7) which lines up relatively well with the water bending overtone in the $1A\cdot D_2$ VPT2 spectrum.

The acetate-specific features assigned in the $n = 0$ spectrum are also present in the simulations for both $n = 1$ isomers represented in Figure 5, giving assignments for peaks b_9 (antisymmetric carboxylate stretch;

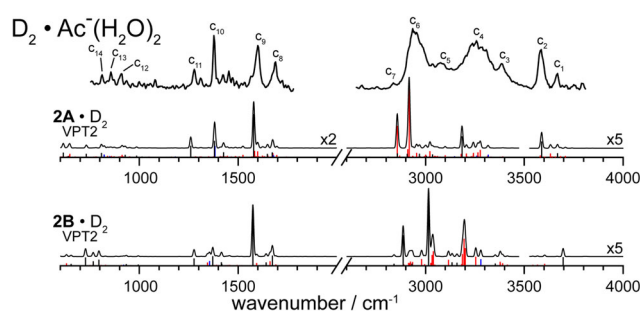


Figure 6. Comparison of the IRPD spectrum of D_2 -tagged $Ac^-(H_2O)_2$ (top) to the VPT2 simulations for the two lowest-energy D_2 -tagged isomers, $2A\cdot D_2$ and $2B\cdot D_2$ (bottom). The stick spectra show fundamental transitions, overtones, and combination bands as black, blue, and red sticks, respectively, and the solid black traces show a convolution of each spectrum with a 15 cm^{-1} FWHM Gaussian lineshape. The $4000\text{--}3500\text{ cm}^{-1}$ regions of both simulated spectra and the $2000\text{--}600\text{ cm}^{-1}$ region of the $2A$ spectrum have been vertically scaled by the indicated factors for clarity.

calc. 1581 cm^{-1} , exp. 1600 cm^{-1}), b_{10} (symmetric carboxylate stretch; calc. 1377 cm^{-1} , exp. 1359 cm^{-1}), and b_{11} (OCO bend; calc. 879 cm^{-1} , exp. 885 cm^{-1}). The water bending fundamental is identified at around $\sim 1700\text{ cm}^{-1}$, corresponding to peak b_8 in the experimental spectrum. An additional water-specific feature is tentatively identified in the $< 1000\text{ cm}^{-1}$ portion of the spectrum (b_{12}), where the $1A\cdot D_2$ harmonic simulation shows a fundamental transition for a water wagging mode involving motion of the shared hydrogen atoms out of the plane formed by the hydrogen-bonded substructures. As is the case in the $n = 0$ VPT2 spectrum, substantial intensity is found for the CH_3 inversion mode that is not observed experimentally, corresponding to the intense simulated peak at $\sim 1220\text{ cm}^{-1}$.

5.3. $n = 2$

VPT2. Figure 6 compares the IRPD spectrum for the $n = 2$ anion to the VPT2 spectra of the two lowest-energy isomers $2A\cdot D_2$ and $2B\cdot D_2$. The presence of two isolated peaks (c_1, c_2) in the free-OH stretching region suggests that isomer $2A$ is the dominant contributor to the spectrum. Based on this comparison, c_1 corresponds to the free OH stretching mode of the AD water molecule (calc. 3668 cm^{-1} , exp. 3665 cm^{-1}), and c_2 corresponds to distortion of the donor OH moiety which participates in the water-water hydrogen bond (calc. 3588 cm^{-1} , exp. 3585 cm^{-1}).

The experimental results are substantially broadened for frequencies between 3500 and 2600 cm^{-1} , though tentative assignments can be made. Peak c_3 may correspond to an overtone of one of the water bending modes,

which appear at frequencies of 3319 and 3260 cm^{-1} in the VPT2 spectrum (versus the experimental value of 3396 cm^{-1}), though there are also numerous combination bands involving the ion-DD OH stretch which could give rise to this peak. Peak c_4 largely consists of the ion-DD OH stretching fundamental (calc. 3186 cm^{-1} , exp. 3260 cm^{-1}). The VPT2 transitions that give rise to peaks c_5 and c_6 appear to be numerous combination bands involving the ion-AD OH stretching mode and various low-frequency modes. Peak c_6 likely includes some contribution from the CH stretching fundamentals, though the VPT2 intensities show that the OH stretching combination bands are substantially more intense. Peak c_7 roughly lines up with the lowest-frequency CH stretching fundamental (calc. 2907 cm^{-1} , exp. 2840 cm^{-1}), and the higher-frequency CH stretches likely contribute to the $c_5 - c_6$ range of features, though their calculated intensities indicate that the OH stretching modes dominate the observed transitions. Thus, whereas the $n = 1$ spectrum shows clearly separated CH and OH stretching regions, the VPT2 results indicate that the CH stretching region is largely obscured by OH stretching vibrational signatures for the $n = 2$ anion.

In the fingerprint region of the $n = 2$ IRPD spectrum, comparison to the $2\mathbf{A}\cdot\text{D}_2$ VPT2 spectrum allows for the assignment of the water bending mode (c_8) as well as both carboxylate stretching fundamentals (c_9 and c_{10}), as summarised in Table 3. These assignments are consistent with those made in this frequency range of the $n = 0$ and $n = 1$ spectra. Both VPT2 spectra show a relatively intense feature at $\sim 1300 \text{ cm}^{-1}$ that corresponds to a CH_3 inversion mode, providing assignment of peak c_{11} ; though this transition shows strong intensity in all VPT2 results provided in the current work, the $n = 2$ anion is the only one which shows this feature experimentally. While the intensities of features in the $< 1000 \text{ cm}^{-1}$ portion of the $2\mathbf{A}\cdot\text{D}_2$ spectrum are substantially lower than expected based on experiment, the VPT2 frequencies in Table S7 show that the OCO bending frequency (928 cm^{-1}) as well as those of two H_2O wagging modes (808 and 731 cm^{-1}) provide reasonable agreement with experimental results. It should be noted that the VPT2 spectrum for $2\mathbf{B}\cdot\text{D}_2$ is similar to that of the lower-energy isomer in terms of peak positions, but differs in the relative intensities of different transitions.

BOMD. We now consider the IR spectrum derived from the BOMD trajectories for the $n = 2$ anion where the initial binding motif is preserved over the 10 ps dynamical time frame (Figure S5). Given the observed tendency of the $2\mathbf{B}$ anion to convert to the lower-energy isomer in the BOMD simulations, we restrict our considerations to the IR spectrum for isomer $2\mathbf{A}$,

Table 3. Peak positions, widths (cm^{-1}), and assignments for observed features in the IRPD spectrum of the D_2 -tagged $\text{Ac}^-(\text{H}_2\text{O})_2$ anion.

peak	cm^{-1}	FWHM	VPT2	desc.
c_1	3665	19	3668	AD free OH str.
c_2	3585	32	3588	DD free OH str.
c_3	3396	69	3319	HOH bend overtone
c_4	3260	149	3186	DD bound OH str.
c_5	3062	147	–	DD and AD bound OH str.
c_6	2945	82	2857	AD bound OH str.
c_7	2840	30	2907	CH str.
c_8	1686	32	1675; 1650	HOH bends
c_9	1599	25	1580	antisym. carboxylate str.
c_{10}	1379	14	1381	sym. carboxylate str.
c_{11}	1220	13	1261	CH_3 inv.
c_{12}	906	19	928	carboxylate bend
c_{13}	857	16	808	H_2O wag
c_{14}	812	15	731	H_2O wag

Note: Assignments for peaks $c_1 - c_6$ are based on generalised motions obtained from the BOMD trajectories, where HD and HA are used to indicate the water which acts as a donor or acceptor in the water-water hydrogen bond. The corresponding VPT2 energies (cm^{-1}) are also provided.

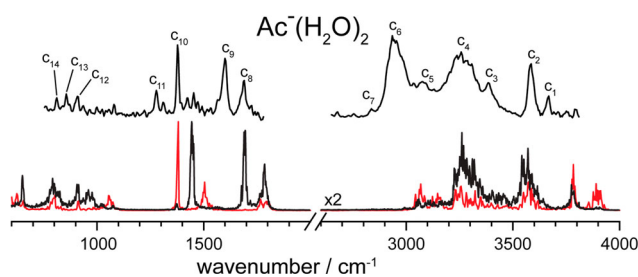


Figure 7. IRPD spectrum of D_2 -tagged $\text{Ac}^-(\text{H}_2\text{O})_2$ (top) compared to the $2\mathbf{A}$ BOMD IR spectrum (bottom, black), where the corresponding vibrational density of states (bottom, red) is also provided; the definitions of these quantities are provided in Figure S5 of the SI. The higher-frequency region of the simulated spectrum has been magnified by the indicated factor for clarity.

in agreement with the assignments based on the VPT2 results. Figure 7 compares the Fourier transforms of the dipole–dipole autocorrelation function (black, IR spectrum) and the nuclear velocity autocorrelation function (red, vibrational density of states) for the $2\mathbf{A}$ BOMD trajectories to experimental results, showing that the general shape of the spectrum is reproduced by theory. The simulated results are fairly blue-shifted relative to experiment in the CH/OH stretching region, likely due to deficiencies of the DFT potential energy surface.

To bolster our assignments of features labelled in Figure 2, we correlate molecular motion calculated from our BOMD trajectories [43] with specific frequencies in the calculated spectral density. In agreement with the VPT2 assignments, bands c_1 (3905 cm^{-1}) and c_2 (3785 cm^{-1}) correspond to the free OH stretch of the AD and the water-bonded OH stretch of the DD water molecule, respectively. The corresponding

Table 4. Vibrational frequencies (in cm^{-1}) extracted from the IRPD spectra of the D_2 -tagged $\text{Ac}^-(\text{H}_2\text{O})_n$ clusters.

	$n = 0$	$n = 1$	$n = 2$
CH str.	2945, 2831	2977, 2942, 2904	2840
antisym. carboxylate str.	1620	1600	1599
sym. carboxylate str.	1341	1359	1379
OCO bend	870	885	906
bound OH str.	–	3600–3000	3500–2900
HOH bend	–	1715	1686
H_2O wag	–	827	857, 812

Note: OH stretching frequencies correspond to those involved with ion-water interactions and are provided as a range due to the relatively broad spectral signatures found for these motions.

nuclear motions are illustrated in Figure S12 of the SI. The vibrational signatures of OH stretches involved in ion-water interactions are found in-between 3700 and 3200 cm^{-1} , with the DD water contributing predominantly above 3500 cm^{-1} (c_3/c_4) and the AD water below $\sim 3400 \text{ cm}^{-1}$. The BOMD simulations suggest a pronounced coupling of the ionic hydrogen bond OH oscillators with low frequency wagging modes, consistent with the prediction of numerous intense combination bands in the VPT2 spectrum and the observation of relatively broad features ($c_3 - c_6$) in the IRPD spectrum. Based on the comparison in Figure 7, the weak feature c_7 at the lower-frequency edge of peak c_6 is correlated with a CH stretching motion (see Figure S12); this peak likely corresponds to the low-frequency end of the CH stretching region, given the absence of structure at lower frequencies in the IRPD results.

6. Discussion

The experiments reported in this work provide information regarding the addition of the first two water molecules to the acetate anion. The 4000 – 2600 cm^{-1} portion of the IRPD spectrum for the $n = 1$ anion (DD binding motif) shows two clearly distinct ranges of structure, which may be separately assigned to the OH (3600 – 3100 cm^{-1}) and CH (~ 3000 – 2800 cm^{-1}) stretching regions, where the CH stretching region shows slightly higher intensity and is not substantially shifted from the corresponding region of the $n = 0$ spectrum (see Table 4). The ratio of integrated intensities of the OH:CH stretching regions is found to be ~ 1.6 from the experimental results in Figure 2; in contrast, the ratio of the sums of OH and CH stretching harmonic intensities is found to be approximately 4. This apparent enhancement of the CH stretching region is likely due to the activity of the D_2 stretching mode, which is predicted to appear in the $< 3100 \text{ cm}^{-1}$ portion of the spectrum given the VPT2 results provided in Table S5.

Addition of the second water to form the AD/DD binding motif results in separation of the OH stretching region into two subsections, corresponding to free/water-water OH stretches (4000 – 3500 cm^{-1}) and ion-water OH stretches (3500 – 2900 cm^{-1}). While the CH stretching fundamentals may contribute some small amount of intensity to peak c_6 , the calculated VPT2 frequencies (3035 , 3005 , and 2907 cm^{-1}) and intensities (harmonic OH:CH ratio ~ 20) indicate that the CH stretching region of the $n = 2$ spectrum is almost entirely obscured by the ion-water OH stretching region, so that only the lowest-frequency CH stretching mode may be identified (peak c_7 , 2840 cm^{-1}). These observations show that addition of the second water results in a substantial increase in the relative intensity of vibrational signatures of OH stretching motion, as well as a broadening of the frequency range over which these transitions occur.

For the acetate anion, each oxygen atom can accept up to three hydrogen bonds, indicating that the first solvation shell of bulk solvated Ac^- consists of six water molecules. The carboxylate stretching frequencies in Table 4 show that as the extent of hydration increases, the symmetric and antisymmetric stretches become more blue- and red-shifted, respectively. This trend is consistent with the values observed for an aqueous solution of sodium acetate, where the symmetric and antisymmetric carboxylate stretch frequencies were found to be 1413 and 1556 cm^{-1} , respectively [23]. Assuming that the splitting in the clusters decreases approximately linearly as more molecules are added, these values suggest that the bulk carboxylate stretch frequencies should be reached at $n \sim 5$, indicating that the frequency shifts observed for the bulk solution are largely due to interactions within the first solvation shell.

IR studies in the CH/OH stretching region of microhydrated nitromethane anions, $\text{CH}_3\text{NO}_2^-(\text{H}_2\text{O})_n$, have shown that the binding motifs of the adsorbed water molecules are similar to those shown in Figure 1 for $n < 3$ [21,45]. As such, similar structural signatures and spectroscopic trends may be identified in the $\text{CH}_3\text{CO}_2^-(\text{H}_2\text{O})_n$ spectra reported here. Both species show an increase in the average CH stretching frequency with increasing n ; this is an indicator of increasing polarisation of the excess charge away from the CH bonds as water molecules are added, due to the delocalisation of the charge throughout the hydrogen bonding network. Additionally, the nitromethane spectra show that as n increases, the CH and OH stretching regions move closer together, due to the aforementioned blue-shifting of the CH stretches as well as the spreading out of the OH stretch fundamentals over a broader range of frequencies. This trend is more pronounced in the acetate data, where

only the lowest-frequency CH stretch can be observed for the $n = 2$ anion due to the broad OH stretching region.

Previously, spectral trends in the vibrational predissociation spectra of microhydrated RCO_2^- and HCO_2^- ions have been considered by Johnson and coworkers in the context of understanding the impacts of metal cations on the spectra of carboxylic acids at water–air interfaces [19,20]. This work found that the addition of the first and second water molecules to the $\text{CD}_3\text{CD}_2\text{CO}_2^-$ anion results in DD and AD/DD binding motifs, respectively, similar to isomers **1A** and **2A** in Figure 1. Due to these similarities, the spectral trends are expected to be similar for these two ions. Figure S13 in the SI plots the carboxylate stretching fundamentals for the two $\text{RCO}_2^-(\text{H}_2\text{O})_n$ series, with the $\text{R} = \text{CH}_3$ values obtained from Tables 1–3 and the $\text{R} = \text{CD}_2\text{CD}_3$ values obtained from the literature [20], showing similar evolution of the symmetric and antisymmetric carboxylate stretching frequencies across the two series of ions.

The spectra presented here may also be compared to results obtained for the microhydrated bicarbonate anion [46], which can be thought of as a carboxylate where $\text{R} = \text{OH}$, to elucidate the impact of the hydrophobicity of the R group on the hydration of RCO_2^- anions. The binding geometry for the addition of the first water molecule is similar between the two anions, where the water molecule forms hydrogen bonds with both deprotonated oxygen atoms of the anion. The reported water bending frequency for the monohydrate is slightly higher in the current results (1715 cm^{-1} for $\text{R} = \text{CH}_3$ versus 1706 cm^{-1} for $\text{R} = \text{OH}$), indicating that the water which binds to the carboxylate group of acetate is more structurally restricted. This may be a consequence of differences in charge delocalisation between the two ions, as the CH_3 group is less likely to pull excess charge away from the CO_2 group. Addition of the second water to the bicarbonate ion results in a DD/DD binding motif, where the second water forms hydrogen bonds with one of the deprotonated oxygen atoms as well as the OH group. While this ion does not take the same AD/DD binding motif as the dihydrate of acetate, a geometry analogous to **2A** was identified as a stable isomer of the $\text{HCO}_3^-(\text{H}_2\text{O})_2$ anion, lying $+4.4\text{ kJ/mol}$ above the lowest-energy structure.

For the $n = 0$ and 1 anions, the harmonic spectra shown in Figures S2–S3 do a fair job of reproducing experiment, particularly in the fingerprint region; in contrast, the harmonic spectrum for the lowest-energy $n = 2$ isomer (Figure S4) does not agree well with experiment. The calculated VPT2 frequencies and intensities give much better agreement for $n = 2$, and result in similar vibrational assignments for $n = 0$ and 1 as may be inferred from a harmonic analysis. For $n = 2$, the VPT2

agreement is particularly good for transitions that have relatively narrow experimental linewidths, but such a treatment cannot account for effects such as dynamical broadening of infrared transitions. The broadening of features in the OH stretching region of the $n = 2$ cluster is reproduced quite well by the BOMD simulations, and the resultant assignments to vibrational motion do not substantially differ between the two methods, though these assignments are not as easily gleaned as those based on a VPT2 analysis as they require a treatment of the generalised normal modes of the ion.

7. Conclusion

Vibrational spectra of the acetate anion complexed with up to two water molecules have been obtained using IRPD spectroscopy of messenger-tagged ions. Vibrational assignments are readily obtained by comparison to VPT2 anharmonic spectra, and these assignments as well as BOMD calculations for the $n = 2$ anion allow for determination of the binding motifs involved in addition of the first two waters to the acetate anion. The current result confirms that the first water molecule adds to the acetate anion in a DD configuration, in agreement with previous results. Addition of the second water leads to formation of the AD/DD water binding motif, involving both ion-water and water-water hydrogen bond formation. The vibrational signatures associated with these two classes of interactions can be clearly distinguished, with the water-water and free-OH stretches appearing at higher frequencies and with narrower linewidths than transitions associated with ion-water OH stretches. Comparison of the ion-water OH stretching regions for the $n = 1$ and $n = 2$ anions shows that addition of the second water results in a red-shift of these vibrational signatures. While the CH stretching region is separately resolved for the $n = 1$ anion, this region is overshadowed by the OH stretching region in the $n = 2$ spectrum, largely due to the broader range of frequencies over which transitions associated with the OH oscillators occur for the larger anion.

Acknowledgements

Y.L. thanks the Alexander-von-Humboldt Foundation for a post-doctoral research fellowship, and L.M.M. acknowledges the Zuckerman STEM Leadership Fellowship. J.A.D. acknowledges NIH grant number S10OD023532 for funding the computational facilities used in this work, and thanks John Kelly for helpful conversations regarding molecular dynamics simulations.

Disclosure statement

No potential conflict of interest was reported by the author(s).

Funding

This work was funded by the US Air Force Office of Scientific Research under grant number FA9550-16-1-0097 and the German Research Foundation DFG (Deutsche Forschungsgemeinschaft) as part of the individual research grant number AS133/3-1 "Spectroscopic Characterization of Salt Dissolution in Microhydrated Cluster Ions and at the Water/Vapor Interface."

ORCID

Sreekanta Debnath  <http://orcid.org/0000-0001-9585-1876>

Ya-Ke Li  <http://orcid.org/0000-0003-1877-1922>

Wieland Schöllkopf  <http://orcid.org/0000-0003-0564-203X>

Daniel M. Neumark  <http://orcid.org/0000-0002-3762-9473>

Knut R. Asmis  <http://orcid.org/0000-0001-6297-5856>

References

- [1] J.J. Max and C. Chapados, *J. Phys. Chem. A* **108**, 3324 (2004).
- [2] J.L. Cornette, K.B. Cease, H. Margalit, J.L. Spouge, J.A. Berzofsky, and C. Delisi, *J. Mol. Biol.* **195**, 659 (1987).
- [3] H. Cid, M. Bunster, M. Canales, and F. Gazitua, *Protein Eng.* **5**, 373 (1992).
- [4] J.L. Finney and A.K. Soper, *Chem. Soc. Rev.* **23**, 1 (1994).
- [5] M. Ide, Y. Maeda, and H. Kitano, *J. Phys. Chem. B* **101**, 7022 (1997).
- [6] F. Franks, *Biophys. Chem.* **96**, 117 (2002).
- [7] H. Schwarz and K.R. Asmis, *Chem. Eur. J.* **25**, 2112 (2019).
- [8] K.R. Asmis and D.M. Neumark, *Acc. Chem. Res.* **45**, 43 (2012).
- [9] M. Okumura, L.I. Yeh, and Y.T. Lee, *J. Chem. Phys.* **83**, 3705 (1985).
- [10] J.M. Lisy, *Int. Rev. Phys. Chem.* **16**, 267 (1997).
- [11] M.A. Duncan, *Int. J. Mass Spectrom.* **200**, 545 (2000).
- [12] W.H. Robertson and M.A. Johnson, *Annu. Rev. Phys. Chem.* **54**, 173 (2003).
- [13] E. Gojlo, M. Smiechowski, A. Panuszko, and J. Stangret, *J. Phys. Chem. B* **113**, 8128 (2009).
- [14] X.-B. Wang, X. Yang, and L.-S. Wang, *Int. Rev. Phys. Chem.* **21**, 473 (2002).
- [15] X.B. Wang, B. Jagoda-Cwiklik, C.X. Chi, X.P. Xing, M.F. Zhou, P. Jungwirth, and L.S. Wang, *Chem. Phys. Lett.* **477**, 41 (2009).
- [16] J.D. Steill and J. Oomens, *J. Phys. Chem. A* **113**, 4941 (2009).
- [17] M. Brümmer, C. Kaposta, G. Santambrogio, and K.R. Asmis, *J. Chem. Phys.* **119**, 12700 (2003).
- [18] A.B. Wolk, C.M. Leavitt, E. Garand, and M.A. Johnson, *Acc. Chem. Res.* **47**, 202 (2014).
- [19] H.K. Gerardi, A.F. DeBlase, X. Su, K.D. Jordan, A.B. McCoy, and M.A. Johnson, *J. Phys. Chem. Lett.* **2**, 2437 (2011).
- [20] J.K. Denton, P.J. Kelleher, M.A. Johnson, M.D. Baer, S.M. Kathmann, C.J. Mundy, B.A.W. Rudd, H.C. Allen, T.H. Choi, and K.D. Jordan, *Proc. Natl. Acad. Sci. U.S.A.* **116**, 14874 (2019).
- [21] W.H. Robertson, E.A. Price, J.M. Weber, J.-W. Shin, G.H. Weddle, and M.A. Johnson, *J. Phys. Chem. A* **107**, 6527 (2003).
- [22] E.M. Myshakin, K.D. Jordan, E.L. Sibert, and M.A. Johnson, *J. Chem. Phys.* **119**, 10138 (2003).
- [23] K. Ito and H.J. Bernstein, *Can. J. Chem.* **34**, 170 (1956).
- [24] D.J. Goebbert, G. Meijer, and K.R. Asmis, *AIP Conf. Proc.* **1104**, 22 (2009).
- [25] D.J. Goebbert, T. Wende, R. Bergmann, G. Meijer, and K.R. Asmis, *J. Phys. Chem. A* **113**, 5874 (2009).
- [26] T.K. Esser, H. Knorke, F. Siro-Brigiano, D.R. Galimberti, K.R. Asmis, M.P. Gaigeot, and J.M. Lisy, *Phys. Chem. Chem. Phys.* **20**, 28476 (2018).
- [27] W. Schöllkopf, S. Gewinner, H. Junkes, A. Paarmann, G. von Helden, H. Bluem, and A.M.M. Todd, *Proc. SPIE* **9512**, 95121L (2015).
- [28] N. Dietl, T. Wende, K. Chen, L. Jiang, M. Schlangen, X.H. Zhang, K.R. Asmis, and H. Schwarz, *J. Am. Chem. Soc.* **135**, 3711 (2013).
- [29] N. Heine and K.R. Asmis, *Int. Rev. Phys. Chem.* **34**, 1 (2015).
- [30] N. Heine and K.R. Asmis, *Int. Rev. Phys. Chem.* **35**, 507 (2016).
- [31] C. Möller and M.S. Plesset, *Phys. Rev.* **46**, 618 (1934).
- [32] R.A. Kendall, T.H. Dunning, and R.J. Harrison, *J. Chem. Phys.* **96**, 6796 (1992).
- [33] M.J. Frisch, G.W. Trucks, H.B. Schlegel, G.E. Scuseria, M.A. Robb, J.R. Cheeseman, G. Scalmani, V. Barone, G.A. Petersson, H. Nakatsuji, X. Li, M. Caricato, A.V. Marenich, J. Bloino, B.G. Janesko, R. Gomperts, B. Mennucci, H.P. Hratchian, J.V. Ortiz, A.F. Izmaylov, J.L. Sonnenberg, Williams, F.Ding, F.Lipparini, F.Egidi, J.Goings, B.Peng, A.Petrone, T.Henderson, D.Ranasinghe, V.G.Zakrzewski, J.Gao, N.Regga, G.Zheng, W.Liang, M.Hada, M.Ehara, K.Toyota, R.Fukuda, J.Hasegawa, M.Ishida, T.Nakajima, Y.Honda, O.Kitao, H.Nakai, T.Vreven, K.Throssell, J.A.Montgomery Jr., J.E.Peralta, F.Ogliaro, M.J.Bearpark, J.J.Heyd, E.N.Brothers, K.N.Kudin, V.N.Staroverov, T.A.Keith, R.Kobayashi, J.Normand, K.Raghavachari, A.P.Rendell, J.C.Burant, S.S.Iyengar, J.Tomasi, M.Cossi, J.M.Millam, M.Klene, C.Adamo, R.Cammi, J.W.Ochterski, R.L.Martin, K.Morokuma, O.Farkas, J.B.Foresman, and D.J.Fox, *Gaussian 16 Rev. B.01* (2016).
- [34] I.M. Mills, in *Molecular Spectroscopy: Modern Research*, edited by K.N.R.a.C.W. Matthews (Academic Press, New York, NY, 1972), pp. 115.
- [35] K. Raghavachari, G.W. Trucks, J.A. Pople, and M. Head-Gordon, *Chem. Phys. Lett.* **157**, 479 (1989).
- [36] R.J. Bartlett, J.D. Watts, S.A. Kucharski, and J. Noga, *Chem. Phys. Lett.* **165**, 513 (1990).
- [37] Y.H. Shao, Z.T. Gan, E. Epifanovsky, A.T.B. Gilbert, M. Wormit, J. Kussmann, A.W. Lange, A. Behn, J. Deng, X.T. Feng, D. Ghosh, M. Goldey, P.R. Horn, L.D. Jacobson, I. Kaliman, R.Z. Khaliullin, T. Kus, A. Landau, J. Liu, E.I. Proynov, Y.M. Rhee, R.M. Richard, M.A. Rohrdanz, R.P. Steele, E.J. Sundstrom, H.L. Woodcock, P.M. Zimmerman, D. Zuev, B. Albrecht, E. Alguire, B. Austin, G.J.O. Beran, Y.A. Bernard, E. Berquist, K. Brandhorst, K.B. Bravaya, S.T. Brown, D. Casanova, C.M. Chang, Y.Q. Chen, S.H. Chien, K.D. Closser, D.L. Crittenden, M. Diedenhofen, R.A. DiStasio, H. Do, A.D. Dutoi, R.G. Edgar, S. Fatehi, L. Fusti-Molnar, A. Ghysels,

- A. Golubeva-Zadorozhnaya, J. Gomes, M.W.D. Hanson-Heine, P.H.P. Harbach, A.W. Hauser, E.G. Hohenstein, Z.C. Holden, T.C. Jagau, H.J. Ji, B. Kaduk, K. Khistyayev, J. Kim, J. Kim, R.A. King, P. Klunzinger, D. Kosenkov, T. Kowalczyk, C.M. Krauter, K.U. Lao, A.D. Laurent, K.V. Lawler, S.V. Levchenko, C.Y. Lin, F. Liu, E. Livshits, R.C. Lochan, A. Luenser, P. Manohar, S.F. Manzer, S.P. Mao, N. Mardirossian, A.V. Marenich, S.A. Maurer, N.J. Mayhall, E. Neuscamman, C.M. Oana, R. Olivares-Amaya, D.P. O'Neill, J.A. Parkhill, T.M. Perrine, R. Peverati, A. Prociuk, D.R. Rehn, E. Rosta, N.J. Russ, S.M. Sharada, S. Sharma, D.W. Small, A. Sodt, T. Stein, D. Stuck, Y.C. Su, A.J.W. Thom, T. Tsuchimochi, V. Vanovschi, L. Vogt, O. Vydrov, T. Wang, M.A. Watson, J. Wenzel, A. White, C.F. Williams, J. Yang, S. Yeganeh, S.R. Yost, Z.Q. You, I.Y. Zhang, X. Zhang, Y. Zhao, B.R. Brooks, G.K.L. Chan, D.M. Chipman, C.J. Cramer, W.A. Goddard, M.S. Gordon, W.J. Hehre, A. Klamt, H.F. Schaefer, M.W. Schmidt, C.D. Sherrill, D.G. Truhlar, A. Warshel, X. Xu, A. Aspuru-Guzik, R. Baer, A.T. Bell, N.A. Besley, J.D. Chai, A. Dreuw, B.D. Dunietz, T.R. Furlani, S.R. Gwaltney, C.P. Hsu, Y.S. Jung, J. Kong, D.S. Lambrecht, W.Z. Liang, C. Ochsenfeld, V.A. Rassolov, L.V. Slipchenko, J.E. Subotnik, V.T. Van, J.M. Herbert, A.I. Krylov, P.M.W. Gill, and M. Head-Gordon, *Mol. Phys.* **113**, 184 (2015).
- [38] W.J. Hehre, R. Ditchfield, and J.A. Pople, *J. Chem. Phys.* **56**, 2257 (1972).
- [39] P.C. Hariharan and J.A. Pople, *Theor. Chim. Acta* **28**, 213 (1973).
- [40] T. Clark, J. Chandrasekhar, G.W. Spitznagel, and P.V.R. Schleyer, *J. Comput. Chem.* **4**, 294 (1983).
- [41] J.-D. Chai and M. Head-Gordon, *Phys. Chem. Chem. Phys.* **10**, 6615 (2008).
- [42] G.J. Martyna, M.L. Klein, and M. Tuckerman, *J. Chem. Phys.* **97**, 2635 (1992).
- [43] G. Mathias and M.D. Baer, *J. Chem. Theory Comput.* **7**, 2028 (2011).
- [44] N. Yang, C.H. Duong, P.J. Kelleher, and M.A. Johnson, *J. Phys. Chem. Lett.* **9**, 3744 (2018).
- [45] J.C. Marcum and J.M. Weber, *J. Phys. Chem. A* **114**, 8933 (2010).
- [46] E. Garand, T. Wende, D.J. Goebbert, R. Bergmann, G. Meijer, D.M. Neumark, and K.R. Asmis, *J. Am. Chem. Soc.* **132**, 849 (2010).